RESEARCH ARTICLE | OCTOBER 10 2025

Pressure-driven crystal symmetry and carrier concentration optimization for superior thermoelectric transport properties in layered $AgCrSe_2$

Special Collection: High Pressure Science 2025

Zheng Bi ; Dianzhen Wang; Yiyang Zhou; Yang Gao ; Jing Zou ; Fuyang Liu; Qiang Tao ; Bin Yang ; Huijuan Yue; Luhong Wang ; Haozhe Liu ; Yan Li ; Pinwen Zhu

Matter Radiat. Extremes 10, 067803 (2025)
https://doi.org/10.1063/5.0293464

Matter and Radiation at Extremes | RESEARCH ARTICLE | pubs.aip.org/aip/mre

Pressure-driven crystal symmetry and carrier concentration optimization for superior thermoelectric transport properties in layered $AgCrSe_2$

Cite as: Matter Radiat. Extremes 10, 067803 (2025); doi: 10.1063/5.0293464
Submitted: 28 July 2025 • Accepted: 22 September 2025 •
Published Online: 10 October 2025

Zheng Bi,[1] Dianzhen Wang,[2] Yiyang Zhou,[1] Yang Gao,[3] Jing Zou,[1] Fuyang Liu,[3] Qiang Tao,[1] Bin Yang,[3] Huijuan Yue,[4] Luhong Wang,[5] Haozhe Liu,[3,a)] Yan Li,[1,a)] and Pinwen Zhu[1,a)]

AFFILIATIONS

[1] Synergetic Extreme Condition High-Pressure Science Center, State Key Laboratory of High Pressure and Superhard Materials, College of Physics, Jilin University, Changchun 130012, China
[2] College of Physics and Electronic Information, Luoyang Normal University, Luoyang 471022, China
[3] Center for High Pressure Science and Technology Advanced Research, Beijing 100094, China
[4] State Key Laboratory of Inorganic Synthesis and Preparative Chemistry, College of Chemistry, Jilin University, Changchun 130012, China
[5] Shanghai Key Laboratory of Material Frontiers Research in Extreme Environments, Shanghai Advanced Research in Physical Sciences, Shanghai 201203, China

Note: Paper published as part of the Special Topic on High Pressure Science 2025.
[a)] **Authors to whom correspondence should be addressed:** haozhe.liu@hpstar.ac.cn; liyan2012@jlu.edu.cn; and zhupw@jlu.edu.cn

ABSTRACT

Phase engineering has proven to be an effective strategy for achieving superior thermoelectric performance, while pressure is an excellent means of expanding the phase space of a material. In this paper, the effect of pressure-induced phase transition on improving the crystal symmetry and enhancing the thermoelectric properties of $AgCrSe_2$ under high pressure and high temperature are reported. A structural phase transition from the low-symmetry $R3m$ phase to the high-symmetry $P\bar{3}m1$ phase is discovered below 1 GPa, which increases band degeneracy and contributes to a high electrical conductivity. For the metallic $P\bar{3}m1$ phase, the electrons surrounding the Se^{2-} anion gradually transfer to the Ag^{+} and Cr^{3+} cations as the pressure increases, decreasing the density of states around the Fermi level and thus optimizing the carrier concentration, thereby increasing the Seebeck coefficient while maintaining a high electrical conductivity. Consequently, an ultrahigh power factor of 864 $\mu W \cdot m^{-1} \cdot K^{-2}$ is achieved at 5 GPa and 297 K. This study provides new insights into improving thermoelectric transport properties by applying physical pressure to enhance crystal symmetry and optimize thermoelectric parameters, and also indicates that phase engineering is a compelling strategy to discover or design novel high-performance thermoelectric materials starting from low-symmetry compounds.

I. INTRODUCTION

Thermoelectric (TE) materials have attracted significant attention owing to their ability to directly convert thermal energy into electrical energy without environmental pollution.[1–3] The TE conversion efficiency can be evaluated by dimensionless figure of merit $ZT = S^2\sigma T/\kappa = PFT/\kappa$, where S is the Seebeck coefficient, σ is the electrical conductivity, T is the absolute temperature, κ is the total thermal conductivity, and $PF = S^2\sigma$ is the power factor. However, the strong coupling relationship between PF and κ makes it a considerable challenge to optimize both simultaneously and make substantial progress in ZT. A significant improvement in ZT has

been achieved through the reduction of thermal conductivity via nanostructuring techniques.[4,5] As the thermal conductivity of some key thermoelectric materials approaches their theoretical minimum, various strategies to enhance the power factor have been explored to further improve the thermoelectric figure of merit,[6] such as carrier concentration optimization, defect engineering, band engineering, entropy engineering, and nanostructuring engineering.[7–12]

High-symmetry materials are generally favored for achieving efficient electron transport, because the abundance of equivalent positions in both real and reciprocal space can produce highly degenerate band edges and symmetry-related multivalley carrier pockets, which support maintaining a high carrier concentration and large density of states (DOS) effective mass m^* in one material.[13] However, high-symmetry materials often have the disadvantage of higher thermal conductivity.[14] Thus, the mainstream and promising thermoelectric materials generally have low symmetry with intrinsically low thermal conductivity. Recently, phase engineering has proven crucial in optimizing carrier transport properties for enhancing TE performance.[15–17] By rationally manipulating the low-symmetry structures of materials and converting them into high-symmetry ones, the inherent conflict between electrical and thermal transport can be mitigated, ultimately optimizing the band structure in a direction favorable to thermoelectric performance. For example, GeTe undergoes a phase transition at 700 K from the low-symmetry rhombohedral structure ($R3m$) to the high-symmetry cubic structure ($Fm\bar{3}m$).[18] By alloying with MnTe, the phase transition temperature of GeTe decreases, which increases the degeneracy of the valence band extrema. This increases m^* from $1.44m_e$ to $6.15m_e$, leading to an improved Seebeck coefficient.[19] However, the introduction of alloying elements can induce carrier scattering, which harms carrier transport properties and consequently limits the optimization of TE performance. An attempt to tune a chalcopyrite structure to a high-symmetry pseudo-cubic form has proven effective in improving thermoelectric performance.[20] $AgBiSe_2$ experiences phase transitions from hexagonal to rhombohedral and then to cubic as temperature increases, ultimately achieving the optimum thermoelectric performance in the cubic phase (ZT = 1.5 at 700 K).[21] Doping with Mg or Ga transforms the monoclinic Cu_2SnSe_3 into a cubic structure. This symmetry enhancement causes the effective mass to increase from $0.8m_e$ to $2.6m_e$ and PF to rise from 4.3 to 11.6 $\mu W{\cdot}cm^{-1}{\cdot}K^{-2}$.[22]

These facts suggest that it would be ideal if a thermoelectric could behave electronically as a high-symmetry material but thermally as a low-symmetry material. $AgCrSe_2$, which has a layered crystal structure consisting of alternating $[CrSe_2]^-$ and interstitial Ag^+ layers repeating along the c axis, possesses an intrinsic low thermal conductivity and a moderately high electrical conductivity. Such a remarkable combination of properties, along with the wide chemical variability of this layered structure, suggests that $AgCrSe_2$ is a promising TE material and is worth further investigation. Many strategies for improving its TE performance have been explored, such as carrier concentration optimization,[23] vacancy engineering,[24,25] modulation doping,[26,27] and nanocomposite engineering.[28] Tang *et al.*[26] employed 3% Sb element doping to achieve a considerable improvement (>50%) in PF (~387 $\mu W{\cdot}m^{-1}{\cdot}K^{-2}$ at 750 K) compared with pristine $AgCrSe_2$. By introducing Ag vacancies into the lattice for carrier concentration optimization, the PF of $Ag_{0.9}CrSe_2$ was elevated to ~550 $\mu W{\cdot}m^{-1}{\cdot}K^{-2}$ at 763 K.[29] However, the persistently low PF remains the main bottleneck limiting further improvement of the TE performance of $AgCrSe_2$. Therefore, efficiently enhancing the PF of $AgCrSe_2$ has become a critical challenge that many researchers are eager to overcome.

In view of this, high pressure may provide the conditions necessary to realize the above task. High pressure can compress crystals, shorten interatomic distances, change the arrangement of atoms, and promote new bonding, thus resulting in phase transitions at room temperature without introducing scattering sources, owing to the unchanged chemical composition.[30] This method opens a portal to a novel world of TE in which plentiful exciting research results have emerged. For example, a pressure-driven topological phase transition occurs in Cr-doped PbSe, leading to simultaneous improvements in its electrical conductivity and Seebeck coefficient, thereby greatly enhancing the power factor and ultimately raising the ZT to 1.7, which is significantly higher than the best observed value to date.[31] A significant enhancement in the PF of $Sb_{1.5}Bi_{0.5}Te_3$ has been observed under pressure, and its ZT exceeds 2, surpassing the highest reported values in bulk materials so far.[32] On this basis, we hope to achieve a highly symmetrical crystal structure at room temperature without introducing scattering sources, thereby ensuring uncompromized carrier transport properties and optimizing TE performance across the entire temperature range.

In the present work, the structural phase transition and carrier transport behavior of $AgCrSe_2$ are examined under high pressure. In addition, the $S(P, T)$ and $\sigma(P, T)$ dependences are investigated using *in situ* measurement techniques under high-pressure and high-temperature (HPHT) conditions. The emerging high-symmetry phase under low pressure exhibits a gapless degenerate semiconductor and increased band degeneracy, indicating enhanced thermoelectric transport properties. In addition, rising pressure promotes the transfer of valence electrons from Se to Ag and Cr, decreasing the DOS near the Fermi level and thus optimizing the carrier concentration, thereby increasing the Seebeck coefficient while maintaining a high electrical conductivity. Finally, the TE performance is significantly improved, owing to the enhanced crystal symmetry and the optimized carrier concentration under HPHT. These results demonstrate a fundamental relationship between the structure and thermoelectric behaviors of $AgCrSe_2$, clarifying the mechanism of coordinated regulation on thermoelectric performance by temperature and pressure.

II. EXPERIMENTAL AND COMPUTATIONAL METHODS

For this experiment, commercial $AgCrSe_2$ powder with a purity of 99.99% was purchased from Beijing Beike New Material Technology Co., Ltd. The sample was sintered by spark plasma sintering (SPS) at 50 MPa and 973 K for 5 min in a vacuum atmosphere. The obtained high-quality dense bulk sample served as the precursor for *in situ* measurement of TE transport properties under HPHT. This technique was reported in our previous studies.[33–35] The assembly for *in situ* measurement of thermoelectric transport properties under HPHT is shown in Fig. S1 (supplementary material).

A symmetric diamond anvil cell (DAC) and a nonmagnetic BeCu alloy DAC with a culet size of 400 μm were used for *in situ* high-pressure X-ray diffraction (XRD) experiments and *in situ* high-pressure Hall-effect experiments, respectively. Pre-indented rhenium gaskets with a drilled 120 μm sample chamber were chosen

for both experiments. The *in situ* high-pressure XRD experiments were conducted at beamline BL15U1 of the Shanghai Synchrotron Radiation Facility (SSRF) with a wavelength of 0.6199 Å. Silicone oil was used as the pressure-transmitting medium.[36] The diffraction data were processed and refined using Dioptas and GSAS-II software. For the Hall experiments, alumina served as the insulation layer, and a 10 μm-thick platinum foil was used as the electrodes. A Lake Shore M91 instrument was used to conduct the Hall experiments, and a magnetic field of 1.5 T was applied to the sample. The pressure was measured using the ruby fluorescence method for both high-pressure experiments.[37] The maximum error for pressure determination in this work is ~0.1 GPa.

First-principles calculations were carried out with the Vienna *Ab initio* Simulation Package (VASP) using the projector-augmented-wave (PAW) pseudopotential method.[38,39] The exchange–correlation functional was handled using the generalized-gradient approximation (GGA) in Perdew–Burke–Ernzerhof (PBE) form,[40] and structural relaxations, total-energy calculations, electronic band-structure calculations, DOS analyses, and Bader charge analyses were performed. A plane-wave cutoff energy of 750 eV was adopted. For $AgCrSe_2$, the valence electron configurations were taken as $4d^{10}5s^1$ (Ag), $3p^6 3d^5 4s^1$ (Cr), and $4s^2 4p^4$ (Se). An 11 × 11 × 5 *k*-point mesh was chosen. During structure optimization, both atomic positions and cell parameters were relaxed until the forces on all atoms were below 0.01 eV·Å^{-1}. A DFT + *U* method with U = 3 eV was applied to the Cr 3*d* electrons to more accurately describe the strong correlation of localized electrons. Finally, by analyzing real-space electron localization function (ELF) maps, we revealed the pressure-induced charge redistribution mechanism and clarified the evolution of the electronic structure of $AgCrSe_2$ under pressure.

III. RESULTS AND DISCUSSION

Ambient-pressure XRD was performed on the $AgCrSe_2$ precursors [Fig. 1(a)], and the pattern was Rietveld-refined with GSAS-II software, giving a residual factor of R_{wp} = 1.927% [Fig. 1(b)]. $AgCrSe_2$ crystallizes in a hexagonal system with space group *R*3*m* and lattice parameters $a = b$ = 3.6802 Å, c = 21.2369 Å, and V = 249.0950 Å^3. The structure exhibits a typical layered character, being composed of alternating $CrSe_6$ octahedra and Ag-ion layers stacked along the *c* axis [Fig. 1(b)].[41–43] To investigate the evolution of the crystal structure of $AgCrSe_2$ with increasing pressure, an *in situ* high-pressure XRD experiment was conducted, and the representative patterns are shown in Fig. 1(a). Surprisingly, the XRD pattern shows noticeable changes at 0.3 GPa, with several new diffraction peaks emerging and some original peaks of the *R*3*m* phase disappearing. This signifies the beginning of a pressure-induced structural phase transition. When the pressure increases to 1.4 GPa, the peaks belonging to the *R*3*m* phase vanish completely and the sample is fully transformed to the high-pressure phase. As the pressure increases further, the new phase gradually stabilizes, and all diffraction peaks shift to higher angles, reflecting the continuous reduction of the unit-cell volume consistent with the typical lattice-compression trend under high pressure. Up to 4.6 GPa, no additional new peaks appear, indicating that only one structural phase transition occurs within this pressure range. To clarify the structural evolution pathway, the XRD pattern at 1.8 GPa was

TABLE I. Lattice parameters of $AgCrSe_2$ under high pressure.

Pressure	a (Å)	c (Å)	V (Å^3)	Space group
1 atm	3.6802(3)	21.2369(2)	249.095(40)	$R3m$ (Z = 3)
0.3 GPa	3.6753(4)	21.2267(1)	248.313(54)	
0.3 GPa	3.6946(4)	6.5949(2)	77.960(17)	
0.9 GPa	3.6845(1)	6.5781(2)	77.337(4)	
1.4 GPa	3.6788(1)	6.5628(3)	76.919(5)	$P\bar{3}m1$ (Z = 1)
1.8 GPa	3.6725(1)	6.5601(3)	76.624(5)	
4.6 GPa	3.6303(3)	6.4795(4)	73.953(13)	

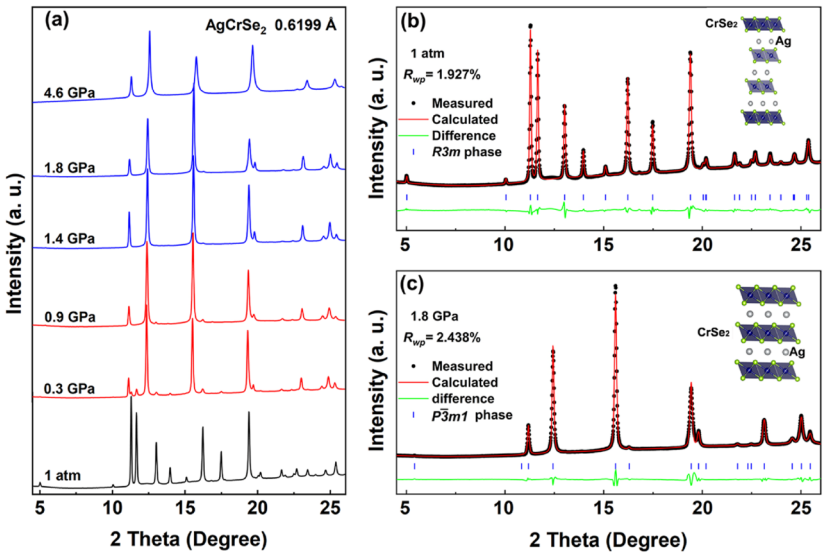

FIG. 1. (a) High-pressure XRD patterns of $AgCrSe_2$ below 5 GPa at room temperature. (b) and (c) Rietveld refinements of XRD patterns at 1 atm and 1.8 GPa, respectively. The red solid line and black circles represent the calculated and experimental data, respectively, and the green lines are the residual intensities. The vertical bars are the diffraction peak positions. The insets show the corresponding crystal structures of $AgCrSe_2$.

analyzed using GSAS-II software. The new phase fits well with the space group $P\bar{3}m1$, as shown in Fig. 1(c), yielding R_{wp} = 2.438% and lattice parameters $a = b = 3.6725$ Å, $c = 6.5601$ Å, and $V = 76.6240$ Å^3. Detailed structural information is given in Table S1 (supplementary material). From the lattice parameters presented in Table I, it is clear that the c axis of $AgCrSe_2$ is greatly compressed during the phase transition. Therefore, the volume collapse during the structural phase transition originates mainly from the compression of the c axis, which also indicates that this structural phase transition is a first-order transition.

For the high-pressure $P\bar{3}m1$ structure, $AgCrSe_2$ still exhibits a distinct layered structure: the $CrSe_6$ octahedra form a robust octahedral network with Cr atoms at the centers and Se atoms at the vertices, while Ag atoms are located between neighboring $CrSe_6$ octahedra, forming a sandwich-like layer structure. After the phase transition, the crystal structure clearly becomes more regular and reaches higher symmetry. Generally, higher crystal symmetry enables highly degenerate band structures, which is beneficial for improving carrier transport properties and thus achieving better TE performance.[13] Given this, we compared the band structures of the ambient-pressure phase ($R3m$) and the high-pressure phase ($P\bar{3}m1$), as shown in Fig. 2. Usually DFT underestimates the bandgap but still accurately reflects its variation under pressure.[44] The $R3m$ phase exhibits a typical semiconductor characteristic, with a bandgap of 0.25 eV [Fig. 2(a)], while the $P\bar{3}m1$ phase shows a gapless band structure [Fig. 2(b)], indicating transport behavior of a degenerate semiconductor.[25,29] It is worth noting that there are five valence bands near the valence band maximum (VBM), suggesting higher valence band degeneracy, thus potentially leading to superior carrier transport.[19,45]

The temperature-dependent electrical conductivity σ and Seebeck coefficient S of $AgCrSe_2$ at ambient pressure were measured, as shown in Fig. S2 (supplementary material). σ gradually increases with rising temperature, while S exhibits the opposite behavior, showing typical semiconductor characteristics, which is consistent with previous experimental results.[25,29,41] The TE transport properties of $AgCrSe_2$ were examined under HPHT and showed a notable variation. First, compared with the ambient-pressure phase ($R3m$), it is evident that the σ of the new high-pressure phase ($P\bar{3}m1$) is significantly enhanced, as shown in Fig. 3(a). For example, at ~300 K, σ increases from 331 S·m^{-1} at ambient pressure (Fig. S2, supplementary material) to 49 268 S·m^{-1} at 1 GPa [Fig. 3(a)]. Besides, over the entire pressure range, the σ of $AgCrSe_2$ decreases with rising temperature, exhibiting typical degenerate-semiconductor transport characteristics.[25,29]

Further analysis of the pressure-dependent σ reveals that it increases slightly between 1 and 2 GPa at room temperature, which should be related to the densification process of bulk $AgCrSe_2$. However, when the pressure increases further, σ starts to decrease. We conducted high-pressure Hall effect measurements to evaluate the room-temperature carrier transport properties under high pressure. As shown in Fig. 3(b), below 2 GPa, the carrier concentration n increases with rising pressure, consistent with the densification process of the sample, leading to a slight increase in σ [Fig. 3(a)]. However, the carrier mobility μ decreases as the pressure rises below 2 GPa [Fig. 3(b)]. This is caused by the typical carrier–carrier scattering in degenerate semiconductors when n is at a high level.[46]

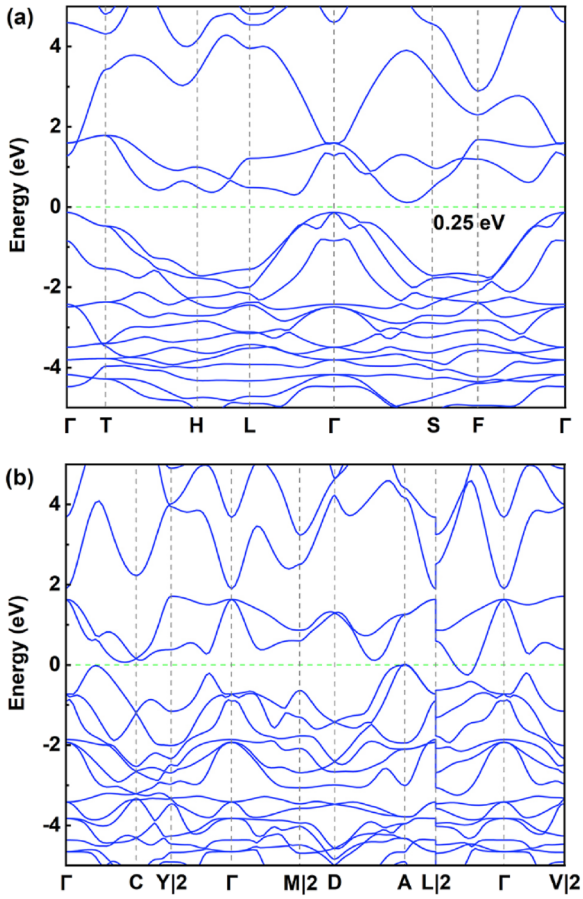

FIG. 2. Calculated band structure of $AgCrSe_2$ at (a) ambient pressure ($R3m$ phase) and (b) 1 GPa ($P\bar{3}m1$ phase).

Above 2 GPa, n starts to decrease, while μ increases. Hence, it can be concluded that the pressure-dependent n determines such behavior of σ under HPHT. The decrease in n between 2 and 5 GPa may be related to the Se-4p orbital charge-transfer mechanism near the Fermi level and will be discussed in more detail later.

Figure 3(c) presents the temperature-dependent S under high pressure. It shows that S is positive, indicating that $AgCrSe_2$ maintains p-type conductive behavior under HPHT. For the $P\bar{3}m1$ phase of $AgCrSe_2$, the pressure effect causes the S to increase at room temperature, reaching a maximum value of 147.54 μV·K^{-1} at 5 GPa. Because of the inherent interdependence of the TE transport parameters, S shows an opposite trend of behavior to σ under HPHT.[47] It is worth noting that owing to the opposite contribution of n to S according to the formula $S = (8\pi^2\kappa_B^2 T/3eh^2)m^*(\pi/3n)^{2/3}$ (where m^* is the DOS effective mass, k_B is Boltzmann's constant, h is Planck's constant, and e is the elementary charge), higher n usually compromises S. Therefore, the decreased n with rising pressure above 2 GPa definitely achieves the optimal n under high pressure. This pressure-induced optimization of n enables a high S while maintaining a high σ, which is favorable for reaching superior PF.

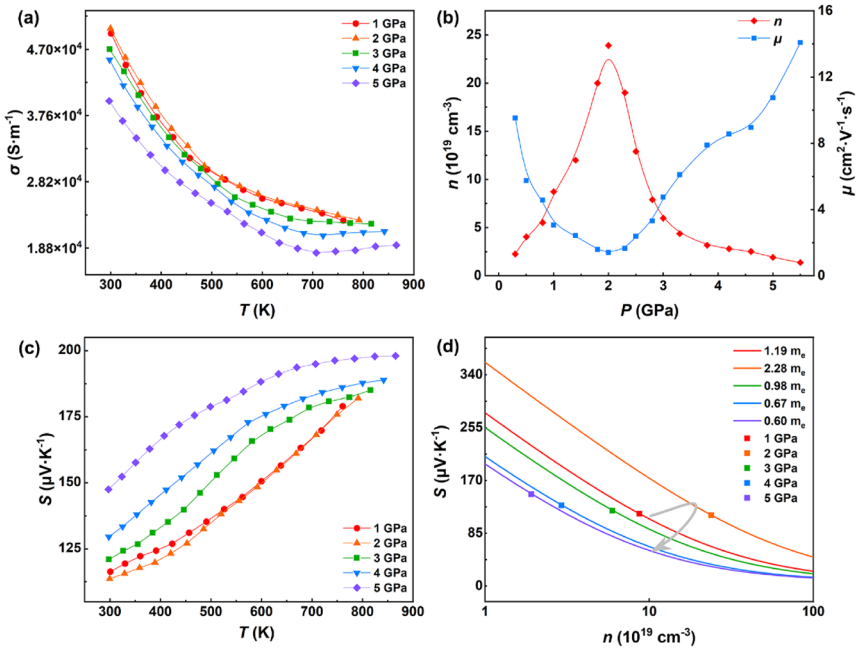

FIG. 3. TE properties of $AgCrSe_2$ under HPHT: (a) electrical conductivity; (b) carrier concentration and mobility; (c) Seebeck coefficient; (d) Pisarenko plot of the absolute value of the Seebeck coefficient vs carrier concentration for $AgCrSe_2$.

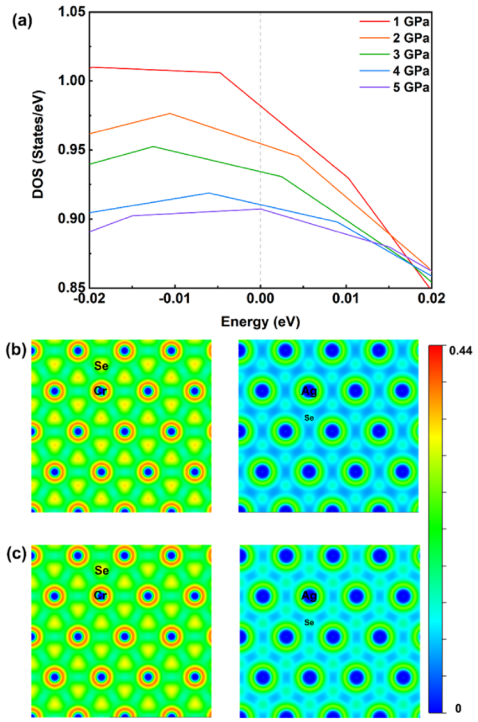

FIG. 4. (a) DOS of the $P\bar{3}m1$ phase of $AgCrSe_2$ under high pressure. (b) and (c) Electron localization function (ELF) in the (001) plane at 1 and 10 GPa, respectively.

Additionally, we analyzed the influence of band structure on carrier transport using a restructured single parabolic band transport model.[48] As shown in Fig. 3(d), the Pisarenko plots show the largest value of m^* ($2.28m_e$) at 2 GPa. The reported m^* at room temperature in $AgCrSe_2$-based TE materials is usually below $0.75m_e$.[23,25] This much higher m^* of the high-pressure phase ($P\bar{3}m1$) of $AgCrSe_2$ is attributed to the highly degenerate band structure, suggesting the great potential of the high-symmetry phase. Above 2 GPa, m^* decreases with increasing pressure, promoting an increase in μ [Fig. 3(b)] and thus maintaining a relatively higher σ. It is worth noting here that although the decrease in m^* is unfavorable for increasing S, the decrease in n [Fig. 3(b)] dominates the increase in S shown in Fig. 3(d).

Critically, the pressure-driven decrease in n is crucial in enhancing carrier transport properties under HPHT. Given this, we performed a detailed analysis of the band structure evolution of the $P\bar{3}m1$ phase of $AgCrSe_2$ under high pressure. As shown in Fig. S3 (supplementary material), with rising pressure, the band structure still keeps the gapless characteristic, leading to such degenerate-semiconductor transport behavior under HPHT as revealed by the temperature-dependent σ [Fig. 3(a)]. However, the calculated total DOS near the Fermi level shows a significant decrease as the pressure increases, as shown in Fig. 4(a). Therefore, the pressure-induced reduction in DOS near the Fermi level causes the decrease in n. This is distinctly different from the behavior of common semiconductors under high pressure. Typically, high pressure fundamentally compresses the crystal structure of a semiconductor, promoting interatomic interactions and charge cloud overlap, which reduces the bandgap and raises n, thereby increasing σ.[49] For example, for the typical layered semiconductor $MoSe_2$, high pressure causes a significant decrease in interlayer spacing and strengthens the interlayer interactions, thereby reducing the bandgap from

0.837 eV at 0 GPa to 0.700 eV at 5.5 GPa and thereby significantly improving n and σ.[33] However, the distinctive feature of our work is that no bandgap was observed in the $P\bar{3}m1$ phase of $AgCrSe_2$ under high pressure (Fig. S3, supplementary material). Thus, there should be other interesting pressure regulation mechanisms dominating this particular behavior of pressure-reduced DOS near the Fermi level.

The DOS of the $P\bar{3}m1$ phase depicted in Fig. S4 (supplementary material) suggests that the valence bands near the Fermi level are mainly composed of the Se 4p orbital. This means that the reduced DOS near the Fermi level with rising pressure [Fig. 4(a)] is closely related to the evolution of electrons in the Se 4p orbital under pressure. Given that, we calculated the electron-localization function (ELF) of the $P\bar{3}m1$ phase at 1 and 10 GPa to observe the transfer mechanism of electrons under pressure. As shown in Fig. 4(b), the valence electrons exhibit clear localization around the Se atoms. As the pressure increases, the electrons around the Se atoms gradually transfer to Ag and Cr atoms [Fig. 4(c)], which leads to the reduction in the DOS near the Fermi level with rising pressure and thereby the decrease in n [Fig. 3(b)]. Consequently, owing to the highly degenerate band structure and optimized carrier concentration under high pressure, an increase in S with maintenance of high σ is guaranteed, ultimately leading to superior PF under HPHT, as shown in Fig. 5(a). It is noteworthy that the reported PFs of $AgCrSe_2$-based TE materials at ambient pressure are relatively low compared with those of many high-performance TE materials. It was reported that the PF of $AgCrSe_2$ at ambient pressure and 700 K is about 225 $\mu W{\cdot}m^{-1}{\cdot}K^{-2}$, and its considerable ZT value depends primarily on its intrinsic low lattice thermal conductivity.[50] Therefore, for $AgCrSe_2$, the key to improving the TE performance is maximizing PF.

In the present study, by applying pressure regulation, an excellent PF as high as 864 $\mu W{\cdot}m^{-1}{\cdot}K^{-2}$ has been achieved for the $P\bar{3}m1$ phase of $AgCrSe_2$ at 5 GPa and room temperature [Fig. 5(a)]. Compared with the previously reported peak value of $R3m$-phase $AgCrSe_2$-based TE materials obtained at room temperature and ambient pressure, the maximum power factor PF_{max} of the $P\bar{3}m1$ phase of $AgCrSe_2$ achieved under high pressure in this work shows significant superiority and even far exceeds its high-temperature

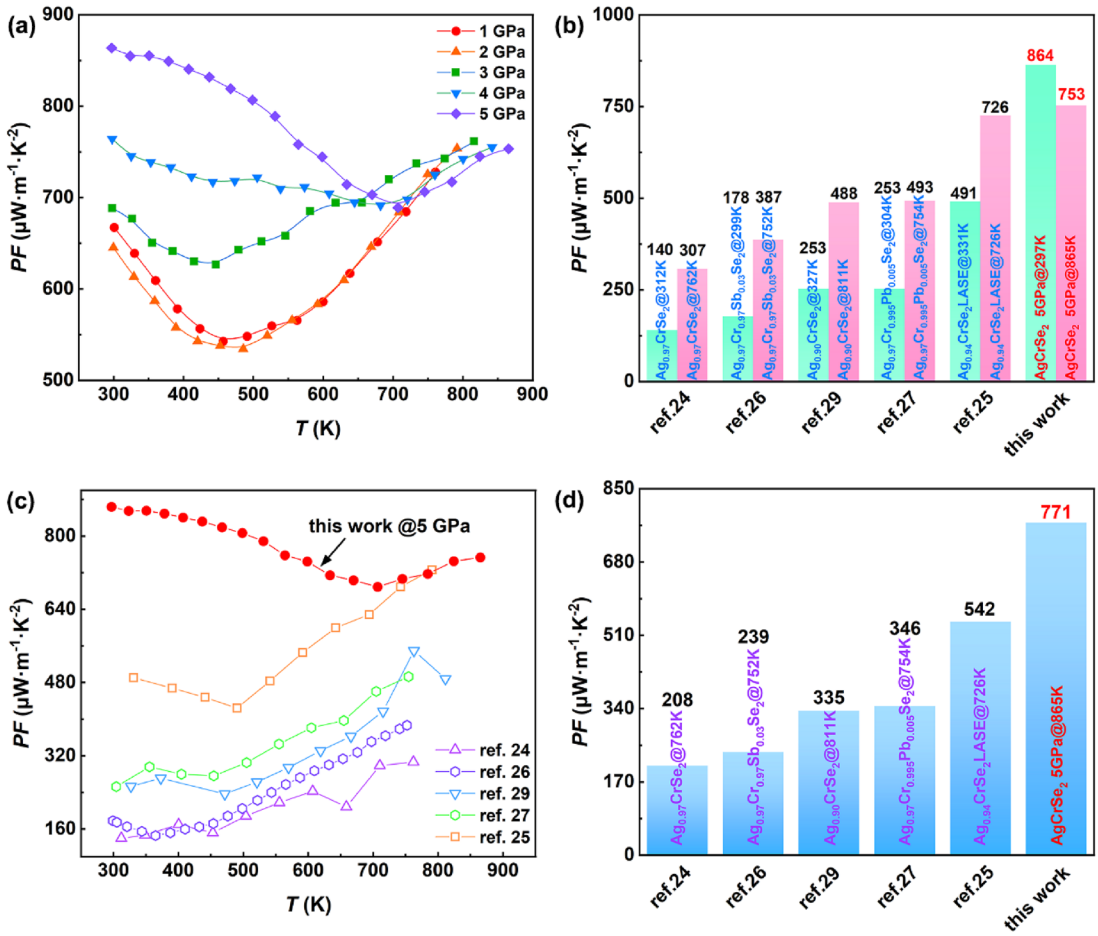

FIG. 5. (a) Power factor of $AgCrSe_2$ under HPHT. (b)–(d) Comparison of maximum power factor, temperature-dependent power factor, and average power factor, respectively, extracted from previously reported $AgCrSe_2$-based TE materials.

value at normal pressure [Fig. 5(b)]. This result greatly compensates for the inherent defect of the low *PF* of $AgCrSe_2$. In addition, the optimal *PF* achieved by phase engineering and high-pressure regulation demonstrates a remarkable advantage in terms of the *PF* across the entire temperature range, as shown in Fig. 5(c). This enables a much higher average power factor PF_{ave} for the high-symmetry $P\bar{3}m1$ phase of $AgCrSe_2$ compared with other reported $R3m$ phases of $AgCrSe_2$-based TE materials [Fig. 5(d)]. These results indicate that combining pressure-driven higher-symmetry phases with pressure-regulated TE parameters is an effective way to improve the thermoelectric properties, especially the *PF* of such materials. It provides a new approach for optimizing the thermoelectric properties of layered or low-dimensional materials. In addition, the characteristics of the transitions in electrical and TE properties suggest that $AgCrSe_2$ is also an excellent candidate for barocaloric cooling applications,[51] which warrants further investigation.

IV. CONCLUSION

By combining high-pressure experimental measurements with first-principles calculations, this study has demonstrated novel dual pressure modulation mechanisms composed of pressure-driven high crystal symmetry and pressure-induced carrier concentration optimization for enhancing TE transport properties in layered $AgCrSe_2$. Specifically, high pressure induces $AgCrSe_2$ to transform from the ambient-pressure $R3m$ phase to a higher-symmetry $P\bar{3}m1$ phase, enabling highly degenerate valence band structures. This promotes a large DOS effective mass to ensure a high Seebeck coefficient. Furthermore, further increase in pressure results in a unique electronic transfer mechanism, namely, transfer of electrons around the Se atoms to Ag and Cr atoms. This leads to a reduction in the DOS near the Fermi level, thereby optimizing carrier concentration, increasing the Seebeck coefficient, and maintaining high electrical conductivity. Finally, such superior carrier transport properties result in a substantial enhancement of the *PF* of $AgCrSe_2$ in the $P\bar{3}m1$ phase under HPHT, compared with previously reported $R3m$-phase $AgCrSe_2$-based TE materials. This study reveals that the application of high pressure effectively overcomes the low-*PF* bottleneck in thermoelectrics with intrinsic low crystal symmetry like $AgCrSe_2$, providing profound insights for the design of high-performance TE materials.

SUPPLEMENTARY MATERIAL

See the supplementary material for a schematic diagram of *in situ* thermoelectric transport properties (Fig. S1), structural information about the $R3m$ and $P\bar{3}m1$ phases for $AgCrSe_2$ (Table S1), the temperature-dependent thermoelectric parameters at ambient pressure (Fig. S2), the calculated band structure of $AgCrSe_2$ with $P\bar{3}m1$ phase at different pressures (Fig. S3), and the calculated total and partial DOS of $AgCrSe_2$ with $P\bar{3}m1$ phase at different pressures (Fig. S4).

ACKNOWLEDGMENTS

The authors are grateful to the staff of BL15U1 of the Shanghai Synchrotron Radiation Facilities and the User Experiment Assist System. This work was supported by the Jilin Province Science and Technology Development Program, China (Grant No. 20250102013JC).

AUTHOR DECLARATIONS

Conflict of Interest

The authors have no conflicts to disclose.

Author Contributions

Zheng Bi, Dianzhen Wang, and Yiyang Zhou contributed equally to this work.

Zheng Bi: Conceptualization (equal); Formal analysis (equal); Investigation (equal); Writing – original draft (equal). **Dianzhen Wang**: Investigation (equal); Methodology (equal); Writing – original draft (equal). **Yiyang Zhou**: Investigation (equal); Software (equal); Writing – original draft (equal). **Yang Gao**: Project administration (equal). **Jing Zou**: Methodology (equal). **Fuyang Liu**: Data curation (equal); Formal analysis (equal). **Qiang Tao**: Data curation (equal). **Bin Yang**: Formal analysis (equal). **Huijuan Yue**: Formal analysis (equal). **Luhong Wang**: Visualization (equal). **Haozhe Liu**: Supervision (equal); Writing – review & editing (equal). **Yan Li**: Conceptualization (equal); Resources (lead); Supervision (equal); Writing – review & editing (equal). **Pinwen Zhu**: Conceptualization (equal); Supervision (equal); Writing – review & editing (equal).

DATA AVAILABILITY

The data that support the findings of this study are available from the corresponding authors upon reasonable request.

REFERENCES

[1] D. Wang, Y. Gao, C. You, J. Cheng, Z. Liu *et al.*, "Enhancement of thermoelectric performance in robust ZnO-based composite ceramics driven by A stepwise optimization strategy," Adv. Funct. Mater. **34**, 2308970 (2024).
[2] D. Beretta, N. Neophytou, J. M. Hodges, M. G. Kanatzidis, D. Narducci *et al.*, "Thermoelectrics: From history, a window to the future," Mater. Sci. Eng.: R: Rep. **138**, 210–255 (2019).
[3] B. Jiang, Y. Yu, J. Cui, X. Liu, L. Xie *et al.*, "High-entropy-stabilized chalcogenides with high thermoelectric performance," Science **371**, 830–834 (2021).
[4] M. S. Toprak, C. Stiewe, D. Platzek, S. Williams, L. Bertini *et al.*, "The impact of nanostructuring on the thermal conductivity of thermoelectric $CoSb_3$," Adv. Funct. Mater. **14**, 1189–1196 (2004).
[5] M. I. Hussein, C. N. Tsai, and H. Honarvar, "Thermal conductivity reduction in a nanophononic metamaterial versus a nanophononic crystal: A review and comparative analysis," Adv. Funct. Mater. **30**, 1906718 (2019).
[6] A. M. Dehkordi, M. Zebarjadi, J. He, and T. M. Tritt, "Thermoelectric power factor: Enhancement mechanisms and strategies for higher performance thermoelectric materials," Mater. Sci. Eng.: R: Rep. **97**, 1–22 (2015).
[7] Y. Pei, Z. M. Gibbs, A. Gloskovskii, B. Balke, W. G. Zeier *et al.*, "Optimum carrier concentration in n-type PbTe thermoelectrics," Adv. Energy Mater. **4**, 1400486 (2014).
[8] Y. Pei, X. Shi, A. LaLonde, H. Wang, L. Chen *et al.*, "Convergence of electronic bands for high performance bulk thermoelectrics," Nature **473**, 66–69 (2011).
[9] Y. Sun, Y. Liu, R. Li, Y. Li, and S. Bai, "Strategies to improve the thermoelectric figure of merit in thermoelectric functional materials," Front. Chem. **10**, 865281 (2022).

[10]D. Wang, Z. Li, Z. Liu, C. You, J. Cheng *et al.*, "Stacking faults stabilize oxygen vacancies at high temperatures to improve the thermoelectric performance of ZnO," J. Alloys Compd. **1005**, 175928 (2024).
[11]R. Chen, P. Qiu, B. Jiang, P. Hu, Y. Zhang *et al.*, "Significantly optimized thermoelectric properties in high-symmetry cubic Cu_7PSe_6 compounds via entropy engineering," J. Mater. Chem. A **6**, 6493–6502 (2018).
[12]G. Tang, W. Wei, J. Zhang, Y. Li, X. Wang *et al.*, "Realizing high figure of merit in phase-separated polycrystalline $Sn_{1-x}Pb_xSe$," J. Am. Chem. Soc. **138**, 13647–13654 (2016).
[13]R. Liu, H. Chen, K. Zhao, Y. Qin, B. Jiang *et al.*, "Entropy as a gene-like performance indicator promoting thermoelectric materials," Adv. Mater. **29**, 1702712 (2017).
[14]Y. Liu, H. Xie, Z. Li, R. dos Reis, J. Li *et al.*, "Implications and optimization of domain structures in IV–VI high-entropy thermoelectric materials," J. Am. Chem. Soc. **146**, 12620–12635 (2024).
[15]H. Zhu, T. Zhao, B. Zhang, Z. An, S. Mao *et al.*, "Entropy engineered cubic n-type $AgBiSe_2$ alloy with high thermoelectric performance in fully extended operating temperature range," Adv. Energy Mater. **11**, 2003304 (2020).
[16]Y. He, T. Day, T. Zhang, H. Liu, X. Shi *et al.*, "High thermoelectric performance in non-toxic earth-abundant copper sulfide," Adv. Mater. **26**, 3974–3978 (2014).
[17]Z. Guo, G. Wu, X. Tan, R. Wang, Z. Zhang *et al.*, "Enhanced thermoelectric performance in GeTe by synergy of midgap state and band convergence," Adv. Funct. Mater. **33**, 2212421 (2023).
[18]M. Hong, J. Zou, and Z. G. Chen, "Thermoelectric GeTe with diverse degrees of freedom having secured superhigh performance," Adv. Mater. **31**, 1807071 (2019).
[19]Z. Zheng, X. Su, R. Deng, C. Stoumpos, H. Xie *et al.*, "Rhombohedral to cubic conversion of GeTe via MnTe alloying leads to ultralow thermal conductivity, electronic band convergence, and high thermoelectric performance," J. Am. Chem. Soc. **140**, 2673–2686 (2018).
[20]J. Zhang, R. Liu, N. Cheng, Y. Zhang, J. Yang *et al.*, "High-performance pseudocubic thermoelectric materials from non-cubic chalcopyrite compounds," Adv. Mater. **26**, 3848–3853 (2014).
[21]C. Xiao, X. Qin, J. Zhang, R. An, J. Xu *et al.*, "High thermoelectric and reversible p-n-p conduction type switching integrated in dimetal chalcogenide," J. Am. Chem. Soc. **134**, 18460–18466 (2012).
[22]L. Hu, Y. Luo, Y. Fang, F. Qin, X. Cao *et al.*, "High thermoelectric performance through crystal symmetry enhancement in triply doped diamondoid compound Cu_2SnSe_3," Adv. Energy Mater. **11**, 2100661 (2021).
[23]M. Tang, J. Li, Y. Wang, H. Gong, Y. Huang *et al.*, "Alloying $Cr_{2/3}Te$ in $AgCrSe_2$ compound for improving thermoelectrics," Appl. Phys. Lett. **118**, 193902 (2021).
[24]M. Tang, Z. Chen, C. Yin, L. Lin, D. Ren *et al.*, "Thermoelectric modulation by intrinsic defects in superionic conductor Ag_xCrSe_2," Appl. Phys. Lett. **116**, 163901 (2020).
[25]Y. Wang, Y. Wang, C. Chen, K. Koumoto, S. He *et al.*, "Remarkable effects of shear-exfoliation and restacking on microstructural texturing and thermoelectric properties of $AgCrSe_2$," J. Alloys Compd. **958**, 170504 (2023).
[26]M. Tang, Z. Chen, X. Guo, F. Zhang, Y. Zhong *et al.*, "Reducing effective mass for advancing thermoelectrics in Sb/Bi-doped $AgCrSe_2$ compounds," ACS Appl. Mater. Interfaces **12**, 36347–36354 (2020).
[27]Y. Wang, F. Zhang, X. Rao, H. Feng, L. Lin *et al.*, "Advancing thermoelectrics by suppressing deep-level defects in Pb-doped $AgCrSe_2$ alloys," Chin. Phys. B **32**, 047202 (2023).
[28]S. Bhattacharya, A. Bohra, R. Basu, R. Bhatt, S. Ahmad *et al.*, "High thermoelectric performance of $(AgCrSe_2)_{0.5}(CuCrSe_2)_{0.5}$ nano-composites having all-scale natural hierarchical architectures," J. Mater. Chem. A **2**, 17122–17129 (2014).
[29]D. Wu, S. Huang, D. Feng, B. Li, Y. Chen *et al.*, "Revisiting $AgCrSe_2$ as a promising thermoelectric material," Phys. Chem. Chem. Phys. **18**, 23872–23878 (2016).
[30]L. Zhang, Y. Wang, J. Lv, and Y. Ma, "Materials discovery at high pressures," Nat. Rev. Mater. **2**, 17005 (2017).
[31]L.-C. Chen, P.-Q. Chen, W.-J. Li, Q. Zhang, V. V. Struzhkin *et al.*, "Enhancement of thermoelectric performance across the topological phase transition in dense lead selenide," Nat. Mater. **18**, 1321–1326 (2019).
[32]D. A. Polvani, J. F. Meng, N. V. Chandra Shekar, J. Sharp, and J. V. Badding, "Large improvement in thermoelectric properties in pressure-tuned p-type $Sb_{1.5}Bi_{0.5}Te_3$," Chem. Mater. **13**, 2068–2071 (2001).
[33]D. Wang, C. You, Y. Ge, F. Wang, X. Wang *et al.*, "Enhanced thermoelectric performance of $MoSe_2$ under high pressure and high temperature by suppressing bipolar effect," Appl. Phys. Lett. **125**, 013903 (2024).
[34]D. Wang, J. Zou, C. You, Y. Ge, X. Wang *et al.*, "Synergistic optimization on Seebeck coefficient and electrical conductivity in 2H-MoS_2 enabled by progressively evolved stacking faults under high pressure and high temperature," Appl. Phys. Lett. **125**, 213903 (2024).
[35]D. Wang, M. Faizan, J. Zhu, W. Quan, Y. Chen *et al.*, "Breaking through the optimization limits of power factor via pressure-decoupled Seebeck coefficient and electrical conductivity," Chin. Phys. Lett. **42**, 066401 (2025).
[36]A. B. Grag, D. Errandonea, P. Rodríguez-Hernández, and A. Muñoz, "$ScVO_4$ under non-hydrostatic compression: A new metastable polymorph," J. Phys.: Condens. Matter **29**, 055401 (2017).
[37]H. K. Mao, P. M. Bell, J. W. Shaner, and D. J. Steinberg, "Specific volume measurements of Cu, Mo, Pd, and Ag and calibration of the ruby R_1 fluorescence pressure gauge from 0.06 to 1 Mbar," J. Appl. Phys. **49**, 3276–3283 (1978).
[38]G. Kresse and J. Furthmüller, "Efficient iterative schemes for *ab initio* total-energy calculations using a plane-wave basis set," Phys. Rev. B **54**, 11169–11186 (1996).
[39]P. E. Blöchl, "Projector augmented-wave method," Phys. Rev. B **50**, 17953–17979 (1994).
[40]J. P. Perdew, K. Burke, and M. Ernzerhof, "Generalized gradient approximation made simple," Phys. Rev. Lett. **77**, 3865–3868 (1996).
[41]U. K. Gautam, R. Seshadri, S. Vasudevan, and A. Maignan, "Magnetic and transport properties, and electronic structure of the layered chalcogenide $AgCrSe_2$," Solid State Commun. **122**, 607–612 (2002).
[42]H. Takahashi, T. Akiba, A. H. Mayo, K. Akiba, A. Miyake *et al.*, "Spin-orbit-derived giant magnetoresistance in a layered magnetic semiconductor $AgCrSe_2$," Phys. Rev. Mater. **6**, 054602 (2022).
[43]S. Kim, J. Zhu, M. M. Piva, M. Schmidt, D. Fartab *et al.*, "Observation of the anomalous Hall effect in a layered polar semiconductor," Adv. Sci. **11**, 2307306 (2024).
[44]T. Ouahrani, R. M. Boufatah, M. Benaissa, Á. Morales-García, M. Badawi *et al.*, "Effect of intrinsic point defects on the catalytic and electronic properties of Cu_2WS_4 single layer: *Ab initio* calculations," Phys. Rev. Mater. **7**, 025403 (2023).
[45]Z. Zhang, H. Yao, X. Jia, X. Wang, X. Li *et al.*, "Band convergence and phonon engineering to optimize the thermoelectric performance of $CaCd_2Sb_2$," Appl. Phys. Lett. **120**, 041901 (2022).
[46]X. Su, S. Hao, T. P. Bailey, S. Wang, I. Hadar *et al.*, "Weak electron phonon coupling and deep level impurity for high thermoelectric performance $Pb_{1-x}Ga_xTe$," Adv. Energy Mater. **8**, 1800659 (2018).
[47]C. Xiao, Z. Li, K. Li, P. Huang, and Y. Xie, "Decoupling interrelated parameters for designing high performance thermoelectric materials," Acc. Chem. Res. **47**, 1287–1295 (2014).
[48]J. Zhu, X. Zhang, M. Guo, J. Li, J. Hu *et al.*, "Restructured single parabolic band model for quick analysis in thermoelectricity," npj Comput. Mater. **7**, 116 (2021).
[49]N. V. Morozova, I. V. Korobeinikov, and S. V. Ovsyannikov, "Strategies and challenges of high-pressure methods applied to thermoelectric materials," J. Appl. Phys. **125**, 220901 (2019).
[50]A. Maignan, E. Guilmeau, F. Gascoin, Y. Bréard, and V. Hardy, "Revisiting some chalcogenides for thermoelectricity," Sci. Technol. Adv. Mater. **13**, 053003 (2012).
[51]A. Aznar, P. Lloveras, M. Romanini, M. Barrio, J. L. Tamarit *et al.*, "Giant barocaloric effects over a wide temperature range in superionic conductor AgI," Nat. Commun. **8**, 1851 (2017).